Kinetics of Calcite Dissolution in CO_2-Saturated Water at Temperatures between (323 and 373) K and Pressures up to 13.8 MPa

Cheng Peng, John P. Crawshaw, Geoffrey C. Maitland, and J. P. Martin Trusler*

Qatar Carbonates and Carbon Storage Research Centre and Department of Chemical Engineering, Imperial College London, South Kensington Campus, London SW7 2AZ, United Kingdom

* To whom correspondence should be addressed. E-mail: m.trusler@imperial.ac.uk

Abstract

We report measurements of the calcite dissolution rate in CO_2-saturated water at pressures ranging from (6.0 to 13.8) MPa and temperatures from (323 to 373) K. The rate of calcite dissolution in HCl(aq) at temperatures from (298 to 353) K was also measured at ambient pressure with *p*H between 2.0 and 3.3. A specially-designed batch reactor system, implementing a rotating disc technique, was used to obtain the dissolution rate at the solid/liquid interface of a single crystal, free of mass transfer effects. We used Vertical Scanning Interferometry to examine the texture of the calcite surface produced by the experiment and the results suggested that at far-from-equilibrium conditions, the measured calcite dissolution rate was independent of the initial defect density due to the development of a dynamic dissolution pattern which became steady-state shortly after the onset of dissolution. The results of this study indicate that the calcite dissolution rate under surface-reaction-controlled conditions increases with increase of temperature from (323 to 373) K and CO_2 partial pressure from (6.0 to 13.8) MPa. Fitting the conventional first order transition state kinetic model to the observed rate suggested that, although sufficient to describe calcite dissolution in CO_2-free HCl(aq), this model clearly underestimate the calcite dissolution rate in the (CO_2 + H_2O) system over the range of conditions studied. A kinetic model incorporating both *p*H and the activity of CO_2(aq) has been developed to represent the dissolution rates found in this study. We report correlations for the corresponding reaction rate coefficients based on the Arrhenius equation and compare the apparent activation energies with values from the literature. The results of this study should facilitate more rigorous modelling of mineral dissolution in deep saline aquifers used for CO_2 storage.

1. Introduction

In recent years, carbon capture and storage (CCS) has emerged as a key technology for limiting anthropogenic CO_2 emissions while allowing the continued utilisation of fossil fuels. Potential CO_2 storage sites include active and depleted hydrocarbon reservoirs, un-mineable coal seams and deep saline aquifers [1]. Of these, the most promising geological formations for safe CO_2 storage are deep saline aquifers because the capacity, integrity and injection economics are most favourable, and the environmental impact can be minimal [2, 3]. Many physical and chemical processes are known to occur both during and after CO_2 injection in saline aquifers, including diagenetic chemical reactions and associated permeability changes [4]. The coupling of physical and chemical processes occurs in various situations, ranging from the near-well-bore region to far in the reservoir, and has consequences for the long-term viability of CO_2 storage [5]. Therefore, it is essential to have a fundamental understanding of the physical and chemical properties of the fluids and minerals, and of the rock-fluid interactions, before implementing CO_2 storage in saline aquifers. Since carbonate minerals are abundant in sedimentary rocks, one of the requirements is to characterise the reactivity of carbonate minerals in aqueous solutions at reservoir conditions [6].

The importance of carbonate dissolution in the (CO_2 + H_2O) system can be understood in terms of its impact on the integrity and stability of both the formation rocks and cap rocks [7, 8]. The chemical interactions between CO_2-acidified brines and the reservoir minerals can influence the porosity and permeability of the formations, resulting in changes in the transport processes occurring during CO_2 storage. Typical examples reported in the literature include formation damage near the injection well and destabilisation of carbonate cements due to the presence of CO_2, either of which could result in premature termination of CO_2-storage operations [9]. Furthermore, literature suggests that mineralisation of CO_2 occurs by a similar mechanism to the reverse process of carbonate dissolution. Hence, information derived from carbonate dissolution studies may be applied to enhance understanding of all aspects of CO_2 storage operations at a given site [10, 11].

Calcite and dolomite are the major carbonate minerals in sedimentary rocks, and calcite is by far the most abundant carbonate mineral in deep-sea sediments [12]. Numerous studies have been performed to understand calcite dissolution rates under various conditions of temperature, pressure and salinity [13-20]. Some of these studies were focused on the more acidic environment, such as acid fracturing for enhanced oil/gas extraction [21, 22]. However, most were performed to evaluate sedimentary-rock and ocean-water chemistry. For CO_2-acidified aqueous systems, the chemical reactions involved during carbonate dissolution have usually been described in terms of up to three parallel reactions occurring at the solid-fluid interface as follows [15-17, 23]:

$$MCO_3 + H^+ \xrightarrow{k_1} M^{2+} + HCO_3^- \quad (1)$$

$$MCO_3 + H_2CO_3^* \xrightarrow{k_2} M^{2+} + 2HCO_3^- \quad (2)$$

$$MCO_3 \xrightarrow{k_3} M^{2+} + CO_3^{2-}. \quad (3)$$

Here, M represents a divalent metal ion (Ca in the present work), $H_2CO_3^*$ is the sum of dissolved molecular CO_2(aq) and H_2CO_3 in the aqueous system, and k_1, k_2 and k_3 are rate coefficients. Plummer [15] suggests that the kinetics of calcite dissolution in the (CO_2 + H_2O) system can be divided into three regimes. In regime 1, dissolution is independent of CO_2 pressure *per se*, dominated by reaction (1) and hence dependent on the system *p*H only. In regime 2, dissolution is dependent on both *p*H and the partial pressure of CO_2 while in regime 3, calcium precipitation begins to play a role. Therefore, the overall carbonate dissolution rate can be described by:

$$r = k_1 a_{H^+} + k_2 a_{H_2CO_3^*} + k_3 , \quad (4)$$

Where a_X is activity of species X. This model has been used in several reservoir simulators; nevertheless, uncertainty remains concerning both the validity of this description and the values of the rate constants that appear in it under the conditions of pressure, temperature, *p*H and ionic strength pertaining to CO_2 storage. One reason for this is the limited amount of literature relating to such conditions. It has also been noted that the high solubility of CO_2 at reservoir conditions could result in significant changes to the activities of reactants and products participating in the dissolution process and alteration of the elementary steps responsible for rate control [12]. Another complexity in many experimental studies of calcite dissolution kinetics is the distinction between the reaction-controlled and mass-transfer-controlled regimes. For the experiments conducted in batch or mixed flow reactors in which only overall reaction rate can be measured, the calcite dissolution rate may be primarily controlled by the hydrodynamic conditions that influence the thickness of the stagnant boundary layer. As a consequence, the observed reaction rates can be very different due to the varying influence of mass transfer resistance. Different values of the rate constants k_1, k_2 and k_3 have therefore been reported in the literature for different temperature and *p*H conditions and a fairly wide range of activation energies have been derived [15, 24, 25]. Since the rate equation (4) is phenomenological, the coefficients and any derived activations energies are best considered as apparent values.

Despite a significant number of studies on calcite dissolution in aqueous solutions, very few experiments have been conducted at high-temperature high-pressure conditions. Pokrovsky *et al*. [26, 27] have measured the dissolution of calcite, dolomite and magnesite at temperatures up to 423 K with pressures up to 5.5 MPa. However, typical CO_2 storage aquifers at depths of 1,000 metres will have pressures of around 10 MPa which may further increase to (12 to 15) MPa with the continuous injection of CO_2 [1]. To our knowledge, no experimental data have been reported at such reservoir-like conditions. Additionally, calcite dissolution in low *p*H conditions (*p*H < 4) have often been studied under mass transfer limited conditions where hydrodynamics are highly influential and the data may not reflect the fluid transport conditions within the porous structure of the saline formation. Furthermore, the review by Morse *et al*. [28] has suggested that much fundamental knowledge is lacking in understanding surface-controlled calcite dissolution reactions. The calcite dissolution data reported by Pokrovsky *et al*. [26, 27] were affected by mass transfer limitations even at the highest speed available in their rotating-disc reactor. Little is known about the influences of temperature and pressure on the calcite dissolution in the surface-reaction-controlled regime. The surface reaction controlled dissolution kinetics can be critical when advection is dominant during

reactive transport process and is the key parameter to be implemented into reactive transport modelling for CO_2 storage simulation. In summary, very few experiments have been conducted at high-pressure and high-temperature reservoir-like conditions that are applicable to CO_2 storage. Furthermore, most of the available data appear to be affected by mass-transfer resistance at the solid-liquid interface and experimental calcite dissolution data in the (CO_2 + H_2O) system under surface-reaction-controlled regime are scattered.

The impact of mass-transfer resistance on the overall dissolution rate can be reduced or eliminated using the rotating disc technique [29]. The transport rate constant (k_t) for the rotating-disk reactor at finite disk rotation speeds is given by

$$k_t = D / \delta , \tag{5}$$

where D is the diffusion coefficient of CO_2 and δ is the diffusion boundary layer thickness (stagnant boundary layer thickness) which in laminar flow is given approximately by the following relation [29-31]:

$$\delta = 1.61 (D / v)^{1/3} (v / \omega)^{1/2} . \tag{6}$$

Here, v is the kinematic viscosity of the fluid and ω is the angular velocity of the disc. Thus, the thickness of the stagnant boundary layer reduces with increase of the rotational speed, resulting in an increase of the flux of solute to the surface for a given concentration gradient. At a sufficiently-high angular velocity, surface reaction becomes the rate determining step and the overall reaction rate obtained experimentally will be free of mass transfer effects. The technique has also been applied to vary the concentration of the reactants and products on the solid surface in a controlled manner and to evaluate the reaction rate, ion diffusion coefficient and the order of reaction [32, 33].

Surface area is another key variable that influences the measured calcite dissolution rate and alternations of surface morphology may result in significant changes of dissolution rate. Holdren and Berner [34] proposed that defect-sites, such as dislocation and fractures, have a higher tendency to dissolve due to the existence of excess surface energy compared to a smooth surface. These observations were subsequently verified with the advent of atomic-scale topographic techniques, such as Atomic Force Microscopy (AFM) and Vertical Scanning Interferometry (VSI) [35-38]. Calcite dissolution rate can be directly calculated from the real-time observation of the topographic changes by using step-retreat velocities and the step densities [39]. Models describing the calcite dissolution kinetics based on those microscopic observations were subsequently proposed to account for the various dissolution rates at different defect sites. However, issues were raised after comparing the macroscopic and microscopic results since, in some cases, both dissolution rates agree whereas, in other cases, orders of magnitude differences were observed [38, 40, 41]. This leads to a further debate on the applicability of the experimental macroscopic and microscopic dissolution rate in reactive transport models since the geometrical surface area strongly depends on the scale at which the process are observed [42].

From the above discussion, we conclude that additional studies are required for calcite dissolution in (CO_2 + brine) systems at reservoir conditions. However, for such studies to be

meaningful, one must first have a thorough understanding of calcite dissolution in the simpler (CO_2 + H_2O) system. Accordingly, the main objective of the present research was to measure systematically the calcite dissolution rate in CO_2 saturated water, free of mass transfer effects, and to quantify the impact of high CO_2 pressure on the dissolution rate and kinetics. In this paper, we described a new batch dissolution reactor system for investigating calcite dissolution under surface-reaction-controlled conditions using the rotating disc technique. We have applied this technique for calcite dissolution in the (CO_2 + H_2O) system at temperatures from (323 to 373) K and pressures up to 13.8 MPa at far-from equilibrium conditions. Our second objective was to probe whether changes in defect densities can result in different calcite dissolution rates in the surface-reaction controlled regime at far-from-equilibrium conditions. Batch-type experiments usually use geometric surface area as an approximation to the reactive surface area and neglect the change of surface morphology. However, the validity of such approximation is still debatable and is highly dependent on the saturation conditions of the solution. Therefore, understanding the impact of surface morphology on "macroscopic" dissolution rate will facilitate more rigorous modelling of mineral dissolution in deep saline aquifers used for CO_2 storage.

2. Experiments

2.1. Material

CO_2 with a specified minimum mole-fraction 0.99995 was supplied by BOC in a liquid-withdrawal cylinder. Pure deionised water with electrical resistivity > 18 MΩ·cm at T = 298 K was produced with a reverse-osmosis apparatus (Millipore) and degassed using an ultrasonic bath before use. Oxygen-free N_2 was supplied by BOC. Hexane and propan-2-ol used in this work for cleaning purposes were purchased from Sigma Aldrich with purities of 0.95 or higher. Sigma Aldrich also supplied 0.01 M HCl(aq), 0.1 M HNO_3(aq) and 0.02 M aqueous 2,6-pyridinedicarboxylic acid. The carbonate samples used in this experiment were cleaved from a single large rhombohedral crystal of Iceland Spar obtained from Bolivia.

2.2. Batch Dissolution Reactors

Figure 1 is a schematic of the three-vessel reactor system used in our carbonate-dissolution experiments. All the wetted metallic parts were made from either titanium or Hastelloy C276, both of which offer resistance to corrosion in concentrated brines at high temperature.

All three reactors were supplied by Parr Instruments Ltd. Reactor 1 permits an aqueous solution to be brought into equilibrium with the mineral of interest in the absence of CO_2; this would corresponded, for example, to the state of formation brine prior to injection of CO_2. Since the focus of this study is dissolution at far-from-equilibrium condition, reactor 1 was not used in the present work. The other two reactors were of the same type (model 4545) with an inner diameter of 8.25 cm, an internal depth of 11.9 cm and a working volume of 600 cm^3. PTFE o-ring seals were used and the maximum working pressure and maximum working temperature were 40 MPa and 523 K, respectively. Each reactor was equipped with an electric heating jacket, operated with a process controller, to regulate the temperature, and a magnetically-coupled stirrer to ensure the homogeneity of the fluid within. A type J thermocouple in a 1/8''

diameter stainless steel sheath, calibrated with an uncertainty of 0.5 K, was installed into each reactor.

The CO_2 pressure in reactors 2 and 3 was controlled by a syringe pump (Teledyne Isco, model 260DM) with a capacity of 260 cm^3, a maximum operating pressure of 52 MPa and a resolution of 0.01 cm^3. Liquid CO_2 was drawn into the pump through a 0.5 µm pore-size particulate filter. The pump cylinder was cooled by passing water at T = 283.15 K from a circulating chiller through a cooling jacket thereby ensuring that the CO_2 remained in the liquid phase within the pump.

As shown in Figure 2, the mineral sample was mounted in a disc-shaped holder that was fitted to the stirrer shaft of reactor 3. The sample holder was fabricated in titanium and the rock sample was held in place by embedding it in a cast disk of epoxy resin (Stycast 2850 FT) which was then fixed in the holder using grub screws. An additional set of removable titanium stirred blades can be seen above the sample holder in figure 2. The original large sample of calcite was cleaved into small rectangles and cleaned using de-ionised water and propan-2-ol before being fixed in the epoxy resin to provide an exposed area for reaction ranging from 100 mm^2 to 200 mm^2. The resin was then cured in an oven for 12 h at T = 323 K prior to being placed into the rock holder, as seen in Figure 2. The resin ensured that the only one face of the sample was exposed to the solution, the dimension of which was measured with callipers.

Reactor 3 was fitted with a simple manual liquid sampling system (comprising valves V12, V13 and V14). This allowed the withdrawal of small samples (around 1.4 mL) of the solution at various times during the reaction for the purpose of compositional analysis. In order to quantify the amount of dissolved carbonate, samples were analysed by ion chromatography (IC). In this study, a Metrohm 790 Personal Ion Chromatography System was employed with a Metrosep C4 column (250 mm $\times$ 4 mm i.d.), a Metrosep C4 pre-column (50 mm $\times$ 4 mm i.d.), and an electrical-conductivity detector with a detection limit to Ca^{2+} of approximately 50 ppb (parts per billion by mass). The eluent was an aqueous solution containing 2×10^{-3} M HNO_3 and 8×10^{-4} M 2,6-pyridinedicarboxylic acid. The IC system was calibrated using a certified standard solution (Sigma Aldrich) containing 10 ppm of Li^+, Na^+, K^+, Ca^{2+} and Mg^{2+} with an uncertainty of less than 0.02 ppm. The samples taken from reactor 3 were first diluted and then placed in an auto-sampler from which several injections were made onto the IC column.

2.3. Experimental procedure

Prior to first use, the entire system was cleaned thoroughly with hexane, propan-2-ol, deionised water, and CO_2 in sequence, repeated several times. To test the purity of the sample, small pieces of calcite were sliced from each cleavage, dissoved in 0.1 M HNO_3, and analysed by ion chromatography. The detection limit for both Ca^{2+} and Mg^{2+} was 50 ppb. For the calcite used in this study, no cation peaks, other than Ca^{2+}, were observed.

At the start of each experiment 300 mL of de-ionised water was loaded into reactor 2, a volume sufficient to ensure that the calcite sample would be fully immersed in the solution once transferred to reactor 3. After closing the system, the sample solution was further degassed using the vacuum pump for 30 min with stirring at room temperature, before pressurising

reactors 2 and 3 with CO_2 and bringing the system to the desired experimental temperature. To ensure the solution in reactor 2 was fully CO_2-saturated, the liquid was stirred at a rotation speed of 200 rpm for at least 4 h after CO_2 was injected at the required temperature and pressure. Following this, the CO_2-saturated liquid was transferred via V7 (at constant pressure and temperature) to reactor 3 in which the calcite sample was continuously rotating at a given angular velocity. The dissolution of the mineral sample was then monitored by periodically sampling the solution in reactor 3 and measuring its composition as detailed above. During the experiment, pressures and temperatures were constantly monitored and logged.

Samples captured in the tubing between valves V13 and V14 were allowed to cool, flushed into a sample bottle using a flow of low pressure nitrogen, and immediately diluted tenfold with deionised water to avoid precipitation. Samples were taken approximately every 5 to 10 min with a total experiment duration of approximately 60 min. The total amount of solution sampled (8-10 samples) did not exceed 5% of the initial volume of solution.

A similar procedure was followed to measure the dissolution of calcite in HCl(aq). In this case, CO_2 was not introduced and the experiment was carried out under nitrogen gas at ambient pressure.

The dissolution rate r of the calcite in reactor 3 was calculated from the calcium ion concentration c as a function of time t as follows:

$$r = (dc/dt)(V/A), \tag{7}$$

where V is the volume of solution in reactor 3 and A is the geometric area of the calcite sample exposed to the solution. In general, (dc/dt) can be estimated from the experimental $c(t)$ curve. In the present work, only the initial rate of reaction was required and this was determined from the $c(t)$ data gathered during typically the first 15 to 20 min of reaction time (3 to 4 data points). This is to minimise the effect of the changes in both the solution *p*H and the geometric surface. A similar procedure was introduced in the study conducted by Alkhaldi et al. [43] where the first 4 data points (total reaction time of 10 min) were used to derive their reaction rate.

3. Results and Discussion

3.1. Calcite dissolution rate in HCl system.

Fig 3 shows an example for the concentration of dissolved calcium in the solution in reactor 3 as a function of time at constant temperature, (ambient) pressure and sample angular velocity. It can be seen that the concentration of Ca^{2+} in solution increased linearly with time over the first 20 min, after which the slope began to decrease. Using the PHREEQC 3.0 software with the Pitzer database [44, 45], it was estimated that the *p*H value of the HCl solution in reactor 3 had increased by less than 0.04 *p*H units during the first 20 min of reaction at all temperature conditions studied. However, as more calcite dissolved in the solution, the final *p*H value of the solution after 60 min elapsed time was estimated to increase by 0.3 to 0.5 units and this increase could significantly retard the dissolution rates, leading to a more flat curve [46].

A total of 47 rotating-disc experiments were carried out in the present work at temperatures from (295 to 353) K in the (HCl + H_2O) system at ambient pressure. Each experiment uses a new calcite cleavage and no sample was reused. The experimental results are summarised in Table 1, where each reaction rate was determined as the average from 2 or 3 experiments under identical conditions. The repeatability of the reaction rate was found to be within ±15 %.

In order to render the mass-transfer resistance negligible, the disc must be rotated sufficiently fast. To find the angular velocity required to achieve this, a series of experiments was performed for calcite dissolution in the (HCl + H_2O) system at T = 353 K. The experimental results, shown in Fig 4, demonstrated that, with increase of ω, the observed reaction rate initially increased and then reached a plateau which we associate with the surface reaction rate without mass transfer resistance. At this temperature, the minimum angular velocity to eliminate mass-transfer effects for calcite dissolution in 0.01 M HCl was around 70 s^{-1} and the dissolution rate was about 0.0033 $mol \cdot m^{-2} \cdot s^{-1}$.

Alkattan *et al*. [47] proposed a mathematical model to describe the overall reaction rate r for calcite dissolution in rotating disc reactor as a function of rotational speed, which may be deduced from Eqs (4 to 6). Their expression is as follows:

$$\frac{1}{r} = \frac{1}{k_1 c \gamma} + \frac{1}{0.62 D^{2/3} \nu^{-1/6} c} \omega^{-1/2}, \tag{8}$$

where c and γ are the concentration and activity coefficient (on a molarity scale) of H^+ in the bulk solution. The model was applied in this study for calcite dissolving in 0.01 M HCl solution at T = 353 K in the non-reaction controlled regime (ω < 70 s^{-1}). Using the solution kinematic viscosity ($\nu = 0.37 \times 10^{-7}$ $mm^2 \cdot s^{-1}$), the diffusion coefficient was estimated to be 7.8×10^{-9} $m^2 \cdot s^{-1}$. This is in reasonable agreement with the value of 9.4×10^{-9} $m^2 \cdot s^{-1}$ estimated by Alkattan *et al*. [47] from their rotating-disk measurements. However, the geometry of our system, with small rectangular samples set off-centre in a disc-shaped epoxy mould, does not conform to the assumptions upon which equation (8) is based. Furthermore, since the Reynolds' numbers (based on the radius of the sample holder) exceeded 10^5 in the plateau region of Fig. 4 it is likely that the flow became turbulent at high rotational speeds rather than being laminar as assumed in the derivation of equation (8). Accordingly, only data gathered at high rotational speeds were used and these were identified as being surface-reaction controlled.

Compton [25] proposed that calcite dissolution kinetics in the surface-reaction-controlled regime in a strong acid at pH < 4 could be modelled as a simple first-order heterogeneous reaction, in which case

$$r = k_1 \cdot \alpha_{H^+}, \tag{9}$$

where k_1 is the rate coefficient appearing in Eq. 8. The dissolution rates of calcite in HCl solution at T = 353 K, ambient pressure, and pH of 2.0 to 3.3 are presented in Fig 5 together with the calculated rate coefficients based on Eq. (9). It can be seen that, while the dissolution rate decreased rapidly with increasing solution pH, all the data are consistent with a single value of the reaction rate constant k_1. The relative uncertainty of each k_1 value was obtained through error propagation based on the uncertainties of r and pH and was found to be around

16 % at 95 % confidence. Fig 6 shows the values of ln(k_1) obtained in this way for calcite dissolution in HCl(aq); the data are plotted as a function of 1/T and conform to the Arrhenius equation. From the slope of the linear regression line and the uncertainties propagated from the k_1 values, the apparent activation energy for calcite dissolution in HCl solution was found to be (16 ± 4) kJ·mol^{-1} at 95% confidence.

A wide range of activation-energy values may be found in the literature and, for dilute solutions under far-from-equilibrium conditions, values of between (20 and 60) kJ·mol^{-1} have been reported [16][33, 48-52]. Sjöberg [16] studied calcite dissolution at *p*H of between 8 and 10 and at temperature of (278.15 to 323.15) K under conditions considered to be mainly surface-reaction-rate controlled, and obtained an activation energy of 35 kJ·mol^{-1}. Later, Sjöberg and Rickard [48] reported an activation energy of (46 ± 4) kJ·mol^{-1} under far-from-equilibrium condition at *p*H of around 8.4 and at temperatures between (274.15 and 335.15) K. These authors used a rotating disc apparatus and analysed the results according to equation (8) to obtain k_1. They did not observe the limiting behaviour seen in our work at high rotational speeds. Lund et al. [33] also used a rotating disc apparatus and reported that at T = 298 K dissolution was mass-transfer limited even at high rotational speed; they concluded from measurements at temperatures between (257.55 and 298.15) K that the apparent activation energy is approximately 60 kJ·mol^{-1}. A smaller values of 35 kJ·mol^{-1} was found by Gutjahr *et al*. [49] using a stirred-vessel apparatus with powdered calcite at neutral to alkaline *p*H. More recently, Finneran *et al*. [50] and Gledhill *et al*. [51] have reported activation energies of (20 ± 2) kJ·mol^{-1} and 20 kJ·mol^{-1} respectively for calcite dissolution in CO_2-saturated saline water; both studied crushed samples at *p*H > 5.4 and stated that the observed rate was reaction controlled. The discrepancies observed between literature sources are substantial and the findings of Sjöberg and Rickard [48] and Lund et al. [33] are qualitatively and quantitatively different from our own. Both of these investigations reported significant mass-transfer limitations in experiments conducted with a rotating-disc apparatus whereas, at high rotational speeds, we found the dissolution rate to be independent of ω indicating that a surface-reaction-controlled limit had been achieved (see Figure 4). Sjöberg and Rickard [48] and Lund et al. [33] both used small discs cut from marble or Icelandic Spar under conditions that appear to have conformed to the assumptions underlying equation (8). On the other hand, our measurements were made at higher Reynolds numbers and this may explain why we found a reaction-controlled limit at high rotational speeds as evidenced in Fig. 4. This factor aside, the differences between the apparent activation energies reported in the literature and in the present study may be associated with the different regimes of *p*H and salinity studied. We speculate that the dynamic steady-state dissolution behaviour, as discussed below for our calcite-CO_2-H_2O studies, may play a role. The abundant, short-lived, small etch pits formed under our experimental conditions lead to more favourable reaction sites, compared to an atomically-flat surface, resulting in a reduction of energy barriers required for dissolution. Similar observations were made by MacInnis and Brantley [20] who reported an apparent activation energy of (27 ± 5) kJ·mol^{-1} for pit deepening and widening, which is comparable with the value reported in this study.

The value of k_1 at T = 298 K estimated from our data is (1.5 ± 0.24) × 10^{-4} m·s^{-1}, which is similar to, but somewhat smaller than, the values reported in the literature. Compton [25] found a reaction rate constant value of (4.3 ± 1.5) × 10^{-4} m·s^{-1} while Plummer et al. reported a value

of 5.0×10^{-4} m·s^{-1}. Arakaki and Mucci [52] deduced a value of 4.0×10^{-4} m·s^{-1} using a surface complexation model. Additionally, from the linear regression of our data (see Fig 6) for k_1 and Eq.(9), the calcite dissolution rates were calculated at T = (298 and 353) K for the *p*H values of 2.03 and 3.19 investigated by Alkattan *et al.* [47] at the same temperature but in the mass-transfer controlled regime. These workers obtained reaction rates of 0.72×10^{-3} mol·m^{-2}·s^{-1} and 1.11×10^{-4} mol·m^{-2}·s^{-1} at *p*H 2.03 and 3.19, respectively, whereas our values are 1.4×10^{-3} mol·m^{-2}·s^{-1} and 2.7×10^{-4} mol·m^{-2}·s^{-1} at the same *p*H and temperature conditions but under surface-reaction-controlled conditions. The greater reaction rates obtained in this work may be consistent with the elimination of mass-transfer resistance [15, 18, 53].

3.2. Calcite dissolution rate in the (CO_2 + H_2O) system.

A total of 80 rotating-disc experiments were carried out in the HCl-free, (CO_2 + H_2O) system at temperatures from (323 to 373) K with pressures up to 13.8 MPa. The concentration-time profiles for all the experiments were similar to those observed in the (HCl + H_2O) system illustrated in Fig 3. The *p*H change during the entire experiment was evaluated by using PHREEQC 3.0 with the Pitzer database and was found to increase monotonically with reaction time. After 20 min, the calculated increase of *p*H ranged from 0.1 to 0.3 *p*H units depending on system temperature and the surface area of the calcite. The more significant increase of *p*H in the (CO_2 + H_2O) system during the first 20 min elapsed time can be attributed to the higher proton concentration of 0.01 M HCl(aq). The large first dissociation constant of HCl (pK_a = -3) compared to H_2CO_3 (pK_a = 6.5) suggests that the *p*H of the (CO_2 + H_2O) system is more susceptible to the increase of HCO_3^- activity in the system [54-56].

In order to account for the minor *p*H change during dissolution, the amount of calcite dissolved was recalculated to the *p*H value at the start of the experiment, assuming the proton-promoted dissolution rates related to this *p*H change is linearly dependent on the H^+ activity change [26] and the relationship can be described by Eqn. 9 at all temperatures:

$$C_{\text{cal}} = C_{\text{meas}} + k_1 \cdot 10^{(\Delta p\text{H})}. \quad (10)$$

Where C_{meas} is the measured concentration of calcite using IC and C_{cal} is the calculated concentration taking into account the change of *p*H. One example of such re-calculated dissolution profile was shown in Fig 7. It can be observed that a linear slope was obtained for the first 20 mins of reaction time, followed by a decline of reaction rate at later times. This change of slope cannot be attributed to the *p*H change since its impact has been corrected. However, the continuous dissolution of calcite will raise the ionic strength of the system, which may also inhibit dissolution as described by Finneran and Morse [50]. The calcite dissolution rate was calculated from the slope of the linear relationship by averaging 2 or 3 experiments under identical conditions. The results are summarised in Table 2 and the repeatability of the reaction rate was found to be within approximately ±15 %.

A series of experiments was also performed to determine the minimum ω required for calcite dissolution in the (CO_2 + H_2O) system at 353 K and 13.8 MPa to eliminate the mass transfer resistance. From Fig 4, it can be seen that the minimum angular velocity required to enter surface-reaction-controlled regime was around 20 s^{-1} for the given conditions and for all future experiments the angular velocity was maintained at 42 s^{-1} or above. The reduction of the

minimum ω compared to the 0.01 M HCl(aq) can be attributed to the slower surface-reaction rate in the (CO_2 + H_2O) system because of the increase of *p*H.

Calcite dissolution rates measured in the (CO_2 + H_2O) system under surface-reaction-controlled conditions are plotted in Fig 8 and span the ranges T = (323 to 373) K and p = (6.0 to 13.8) MPa. It can be seen that the calcite dissolution rate increases with increase of temperature and pressure. Very few studies have been completed on the rate of calcite dissolution in the (CO_2 + H_2O) system at high-temperature high-pressure reservoir conditions. Pokrovsky [26] have recently published a series of studies on calcite dissolution kinetics in the (CO_2 + H_2O) system at temperatures and pressures up to 423 K and 5.5 MPa, respectively; however, their calcite dissolution data were gathered in a mass-transfer-controlled regime. Pokrovsky reported a dissolution rate at T = 373 K and p = 5.0 MPa of 6×10^{-4} mol·m^{-2}·s^{-1} while, in this study, the dissolution rate at the same temperature and p = 6 MPa was 8.2×10^{-4} mol·m^{-2}·s^{-1}. The higher CO_2 pressure in this study could contribute to the rise of reaction rate due to the decrease of *p*H; however, this impact is estimated to be small since the *p*H only decreases by about 0.03 units between (5 and 6) MPa at T = 373 K according to the model of Peng *et.al* [55]. Additionally, the increase of dissolved CO_2 cannot account for the 30% increase of dissolution rate since CO_2 solubility only changed by about 10% from 0.47 mol·kg^{-1} to 0.52 mol·kg^{-1} according to the model proposed by Hou *et al.* [57]. The explanation for the higher reaction rate found in this study is most likely due to the elimination of mass transfer resistance [12]. Similar behaviour was also observed when comparing the values obtained in this study with the data reported by others [15, 24, 53, 58] at similar *p*H values. The calcite dissolution data reported in this study were systematically higher than the literature data measured in the transport-controlled regime.

3.3. Impact of surface morphology on dissolution rate.

As discussed by Schott et al. [41], macroscopic reaction-rate measurements should be rationalized in the light of microscopic studies of the evolution of surface roughness during the dissolution process. In order to illuminate this aspect of the problem, we used a Wyko NT9100 optical profiler to examine the surface morphology of unreacted and partially-reacted calcite samples. This instrument uses Vertical Scanning Interferometry (VSI) to map the surface profile with nanometre resolution over an area of order 1 mm^2. Figure 9 shows an example of the results obtained by this technique. The unreacted sample, which was cleaved in the normal way, is seen to be almost perfectly flat to the resolution of the instrument. After 10 min elapsed time, etch pits have developed on the calcite surface, aligned with the crystallographic axes. The pit morphology is that of an inverted rhombohedra pyramid, reflecting the underlying symmetry of the calcite crystal [39, 58]. The densely-clustered pits are typically shallow, being (8 to 10) μm deep, and measure (350 to 400) μm along an edge. During the time over which we estimated the reaction rate, the topography remains roughly constant as can be seen by comparing the surface profiles measured after 10 min and 20 min in Fig 9. This situation is similar to that reported by Duckworth and Martin [35]. After 60 min reaction, the rhombohedra pyramid features have disappeared and a roughly etched surface with irregular kinks and deep abysses was found; however, this is well beyond the time during which the reaction rate was evaluated.

Given the regular shape and the size of the etch pits during the first 20 min elapsed time, it was possible to calculate the change in sample surface area from the nearly-atomically-flat initial surface. However, the etch pits are so shallow that the relative change turns out to be less than 0.2 %. This justifies our use of the geometric surface area to evaluate the surface reaction rate constant from the linear concentration-time behaviour observed in the initial 20 min.

In order to determine the influence of initial surface roughness on the observed 'macroscopic' dissolution rate, we studied three additional calcite samples with initially modified surfaces and again used VSI to study the surface profiles both before and after 10 min reaction time (see Figure 10). Samples 1 and 2 were ground and polished on a grinder-polisher (Buehler, model EcoMet Pro 300 with AutoMet 300 Power Head). These treated samples can be seen to have very smooth surfaces prior to reaction. No surface defects are evident on sample 1, whereas very minor defects can be observed on sample 2. The average surface roughness (R_a) was calculated according to:

$$R_a = \frac{1}{n}\sum_{i=1}^{n}\left|y_i\right|, \tag{11}$$

where n represent the number of ordered, equally spaced points along the profile and y_i is the vertical distance from the mean line to the i^{th} data point. The average surface roughness for sample 1 was 123 nm as compared with a value of 56 nm for a cleaved calcite sample. The initial surface condition of sample 3 was obtained by reacting a cleaved crystal in the (CO_2 + H_2O) system at T = 353 K and p = 13.8 MPa for 10 min. As shown in Figure 10, all three samples showed a similar "sawtooth" profile after reaction, with rhombohedra-pyramid-shape etch pits distributed over the surface. The "macroscopic" dissolution rates for the three samples with initially modified surfaces are given in Table 2 together with the elapsed time, saturation state and the dissolution rate at the end of each run. From these results we can conclude that there was no statistically-significant difference between the dissolution rates of fresh-cleaved calcite crystals and samples that underwent various pre-treatments. This observation supports the hypothesis that the density of etch pits on the surface rapidly evolves to a dynamic steady state that, under the conditions of our experiment, prevails for at least 20 min during which the rate of dissolution is constant and independent of modest initial roughness. The pristine cleaved surface may well exhibit a different surface reaction rate but the transition to the pitted structure appears to be so rapid that it cannot be measured in our experiments.

This dynamic steady-state dissolution behaviour during the first 20 min elapsed time has also been reported by Macinnis and Brantley [20]. They measured the calcite dissolution rate in the surface-reaction-controlled regime and concluded that the threshold to induce such a steady-state dissolution is the formation of the "sawtooth" surface morphology, which is similar to the surface condition observed in this study. Once the steady state is reached, there is for some time little change in the morphology of the surface or in the dissolution rate with increasing dislocation density [20]. The insignificant impact of defect density on dissolution rates can be attributed to the low Gibbs free energy (ΔG) of the overall calcite dissolution reactions at the conditions investigated in this study. Here, ΔG is defined as:

$$\Delta G = RT\ln\Omega \quad (12)$$

where Ω is the saturation state and can be defined as:

$$\Omega = \frac{\alpha_{Ca^{2+}}\alpha_{CO_3^{2-}}}{K_{sp}} \quad (13)$$

where K_{sp} is the solubility product of calcite. Luttge [37, 59] has studied the impact of surface defect density on mineral dissolution rate and concluded that the impact of etch pits development is dependent on the ΔG value. Teng [60] further developed the theory and extended the discussions to the far-from-equilibrium saturation conditions, in which ΔG is less than -12 kJ·mol^{-1}. They conclude that under such conditions, etch pits are able to form spontaneously on calcite surfaces without the presence of crystal defects. The unassisted and spontaneous two-dimensional pit nucleation events outnumbered those formed from pre-existing defect sites. As a result, when ΔG is less than -12 kJ·mol^{-1}, the effect of dislocation density on calcite dissolution rates is insignificant [36]. In this study, ΔG for all the conditions studied was between -20 kJ·mol^{-1} and -27 kJ·mol^{-1} after 20 min elapsed time. Similar conclusions were supported by Blum [61] and Schott et al[62]. Blum investigated quartz dissolution at far-from-equilibrium conditions and summarised that the dissolution rates of the high and low dislocation density quartz were indistinguishable in both distilled water at 80°C and in 0.2 M HF at 295 K. Schott et al. [62] have reported calcite dissolution for both strain and unstrained samples and noticed that dislocation only plays a dominant role in enhancing calcite dissolution when a critical defect density is reached.

3.4. Impact of CO_2 pressure on calcite dissolution rate

The majority of published calcite dissolution studies, whether macroscopic (*e.g.* using batch or mixed-flow reactors) or microscopic (*e.g.* using AFM), have investigated low CO_2 partial pressure conditions, ranging from 0.04 kPa to 100 kPa ([14, 15, 26, 46]). It is typically found that the impact of dissolved CO_2 is very limited under such conditions, especially when the solution *p*H is low [60]. As a result, the first term in Eq. (4) dominates and the rate equation simplifies to Eq. (9) [13, 53]. However, this situation may not prevail at CO_2 storage reservoir conditions where the partial pressure of CO_2 can range up to 10 MPa ([2, 6]), leading to an almost 100 fold increase in dissolved CO_2 [63]. Due to the low *p*H conditions of the solution, the majority of the dissolved CO_2 remains as CO_2 (aq) [64] and its impact on the calcite dissolution rate can be significant.

The recent study by Pokrovsky [27] has shown that the impact of CO_2 can be very large at higher pressure. However, this increase was mainly attributed to the *p*H drop during CO_2 dissolution. The calcite dissolution rate increased by a factor of 8 when the CO_2 pressure increased from (0.1 to 2.5) MPa. However, this dependence did not persist beyond 2.5 MPa partial CO_2 pressure. In the study reported here, we have observed a continuous increase of the dissolution rate with increasing CO_2 pressure on all four isotherms studied. This increase in the dissolution rate cannot be entirely attributed to the decrease in *p*H. For example, at T = 373 K，the calcite dissolution rate increased nearly two-fold as the pressure increased from (10 to 13.8) MPa, while the *p*H only deceased by 0.04 units. To analyse this behaviour

further, the *p*H of the bulk solution was calculated using the empirical model proposed by Peng *et al.* [55] and $\ln(r / \alpha_{H^+})$ was evaluated at every conditions studied. It can be seen that $\ln(r / \alpha_{H^+})$ is not independent of pressure at constant temperature and that it is systematically greater than found for calcite dissolution in HCl(aq). Hence it is clear that a single first-order heterogeneous reaction does not account for the calcite dissolution rates observed in the (CO_2 + H_2O) system at the temperatures and pressures of interest in this work. Instead, the first two terms in Equation (4) both appear to play a significant role.

The kinetics of calcite dissolution have typically been described using the classic transition-state-theory (TST) which leads to equation (4). However, recent studies have suggested some limitations of such a modelling approach, particularly at the saturation regime in which the dissolution rate (*r*) is highly non-linearly depended with the Gibbs free energy (Δ*G*) [37]. Various models have therefore been proposed to correlate the sigmoidal trend in the dependence of *r* upon Δ*G*. Other models based on experiments using microscopic measurements were also proposed and a surface energy spectra approach was suggested to describe the reaction kinetics [38]. However, the TST-derived rate laws are still preferred for implementation in geochemical modelling codes describing rock-fluid interaction, due to their simplicity and the large number of published rate constants data [41]. Additionally, Teng has recently proposed that the TST model is able to depict the relation between *r* and Δ*G* when the system Δ*G* falls from its extrema (-12 $kJ \cdot mol^{-1}$) [36]. Finally, the lack of integration on the number and the distribution of reactive sites into the TST-based kinetics model may be overcome by using crystal surface roughness as a proxy [41]. Hence, in this paper, we continued our analysis based on Eq. 4. to quantify the impact of high CO_2 partial pressure on calcite dissolution kinetics.

The species denoted $H_2CO_3^*$ in reaction (2) is the sum of dissolved molecular CO_2(aq) and H_2CO_3 in the aqueous system and the overall equilibrium for the bicarbonate system can be described as follows [65, 66]:

$$CO_2 + H_2O = H_2CO_3^* = H^+ + HCO_3^- \quad (14)$$

The small dissociation constant of $H_2CO_3^*$ ($10^{-2.5}$ to 10^{-3}) and the relatively low *p*H under investigation indicates that the equilibrium is strongly in favour of CO_2 (aq) [65, 66]. Hence, in our analysis, the activity of $H_2CO_3^*$ ($\alpha_{H_2CO_3^*}$) was approximated by the activity of dissolved CO_2 (α_{CO_2}), which was obtained from the correlation proposed by Hou *et al.* [57]. Additionally, since k_3 is typically on the order of 10^{-7} $mol \cdot m^{-2} \cdot s^{-1}$ [15, 24, 58], reaction (3) was omitted. The rate constant k_1 was obtained from the present kinetic data for calcite dissolution in HCl, leaving k_2 to be determined from the surface dissolution rates observed in the (CO_2 + H_2O) system. The resulting values of $\ln k_2$ are plotted against inverse temperature in Fig 12 and exhibit a good linear relationship, essentially independent of pressure. Taking the standard uncertainties of *r*, k_1, *p*H and α_{CO_2} into consideration, the overall standard uncertainty of k_2 (u_{k2}) with a 95% confidence level was calculated from the relation

$$\left(\frac{u_{k_2}}{k_2}\right)^2 = \left\{\left(\frac{u_r}{r}\right)^2 + \left[\left(\frac{u_{a_{H^+}}}{a_{H^+}}\right)^2 + \left(\frac{u_{k_1}}{k_1}\right)^2\right]^{0.5}\right\}^2 + \left(\frac{u_{a_{CO_2}}}{a_{CO_2}}\right)^2 \quad (15)$$

and was found to be less than 20%. Extrapolation of the linear fits shown in Fig 12, gave k_2 = (3.0 ± 0.5) × 10^{-7} m·s^{-1} at T = 298.15 K. Similar values have been reported in the literature. Plummer *et al.*[15] found k_2 = 3.4 ×× 10^{-7} m·s^{-1} while Chou *et.al* [24] reported a value around 5 × 10^{-7} m·s^{-1} based on measurements in a fluidised bed reactor. The difference between the k_2 value evaluated in this study and the one found by Chou *et al.* could be attributed to the large uncertainty of the value obtained by Chou *et al.* They suggested in their conclusions that the contribution of H_2CO_3* was not important under their experimental conditions. Teng [36] and Giudici [67] have recently measured dissolution rates for calcite on a microscopic scale using AFM under surface-reaction-controlled, far-from-equilibrium, conditions. Using equation (4) as the kinetics model, with k_3 neglected and the values of k_1 and k_2 proposed in this study, we find very good agreement with the dissolution rates reported by Teng and Giudici. Teng reported a dissolution rate of 4.0 × 10^{-7} mol·m^{-2}·s^{-1} at T = 298 K and ambient pressure while the value calculated from our model is (3.7 ± 0.7) × 10^{-7} mol·m^{-2}·s^{-1} at the same temperature and pressure. Giudici found a dissolution rate of 2.3 × 10^{-7} mol·m^{-2}·s^{-1} at T = 295 K and ambient pressure conditions, while our calculated value is (1.8 ± 0.36) × 10^{-7} mol·m^{-2}·s^{-1}.

4. Conclusions

In the present study, calcite dissolution experiments have been performed in CO_2-saturated H_2O at four temperatures from (323 to 373) K at pressures in the range (6.0 to 13.8) MPa, and also in HCl(aq) over a similar temperature range. A specially-designed batch reactor system, implementing the rotating-disc technique, was used to eliminate mass-transfer resistance and access the reaction rates under surface-reaction-controlled regime at far-from-equilibrium conditions. Examination of the calcite dissolution rate in both CO_2-saturated water and aqueous HCl portrays the limitations of using a single first-order heterogeneous reaction equation to predict the calcite dissolution rate, particularly for (CO_2 + H_2O) system at elevated temperatures and pressures.

Furthermore, it was found in this study that CO_2-promoted dissolution can play a significant role in the kinetics of calcite dissolution. The calcite dissolution rates in the (CO_2 + H_2O) system obtained in this study increased with the increase of CO_2 partial pressure. A rate equation representing parallel reactions involving H^+ and CO_2(aq) was shown to provide a good account of the data, and the activation energies determined for these two reactions were found to be in reasonable agreement with the literature. The calcite dissolution rate calculated using the proposed kinetics model has shown good consistency with other “macroscopic” data from rotating-disc reactors and “microscopic” studies using AFM.

Additionally, the evolution of surface morphology was evaluated during the calcite dissolution process using VSI to study the effect of initial defect conditions on the calcite dissolution rate. A comparison of the measured rates for several calcite samples that underwent various pre-treatment steps showed little distinctions between the samples despite the difference in initial

defect density. The “sawtooth” surface topography and the rapid emergence of a dynamic steady state dissolution behaviour suggest a layer-by-layer dissolution behaviour along the calcite surface. This supports the conclusions of Teng [36] that, at far-from-equilibrium conditions, initial defect density does not affect the calcite dissolution rate. The dissolution rate data and the activation energy parameters proposed in this study should facilitate more rigorous modelling of mineral dissolution in deep saline aquifers used for CO_2 storage.

5. Acknowledgments

We gratefully acknowledge the funding of QCCSRC provided jointly by Qatar Petroleum, Shell, and the Qatar Science & Technology Park.

Table 1: Calcite dissolution rate *r* in the (CO_2 + H_2O) and (HCl + H_2O) systems at temperatures *T*, pressure *p* and angular velocities *ω*.

Dissolution Media	*T*	*p*	*ω*	*r*	Saturation Index (SI)[a]	Gibbs Free Energy (Δ*G*)	*p*H of the bulk solution [b]
	K	MPa	s^{-1}	$mol \cdot m^{-2} \cdot s^{-1}$		$kJ \cdot mol^{-1}$	
HCl (0.01 M)	353.15	0.1	31	0.0015	-9.10	-61.52	2.08
HCl (0.01 M)	353.15	0.1	42	0.0020	-9.23	-62.40	2.08
HCl (0.01 M)	353.15	0.1	63	0.0028	-8.72	-58.95	2.08
HCl (0.01 M)	353.15	0.1	73	0.0032	-9.01	-60.91	2.08
HCl (0.01 M)	353.15	0.1	84	0.0032	-8.50	-57.47	2.09
HCl (0.01 M)	353.15	0.1	94	0.0032	-11.27	-76.19	2.08
HCl (0.01 M)	331.15	0.1	73	0.0032	-9.78	-62.00	2.07
HCl (0.01 M)	323.15	0.1	73	0.0025	-9.68	-59.88	2.06
HCl (0.01 M)	316.15	0.1	73	0.0023	-9.87	-59.74	2.06
HCl (0.01 M)	302.15	0.1	73	0.0020	-10.08	-58.31	2.03
HCl (0.01 M)	294.15	0.1	73	0.0015	-10.28	-57.89	2.00
HCl (6.1×10^{-4} M)	353.15	0.1	73	0.00019	-7.77	-52.53	3.21
HCl (6.6×10^{-4} M)	353.15	0.1	73	0.00020	-7.74	-52.33	3.18
HCl (1.3×10^{-3} M)	353.15	0.1	73	0.00033	-8.42	-56.92	2.90
HCl (1.6×10^{-3} M)	353.15	0.1	73	0.00043	-9.14	-61.79	2.79
CO_2 + H_2O	353.15	13.8	11	0.00092	-3.96	-26.77	3.17
CO_2 + H_2O	353.15	13.8	16	0.00094	-3.55	-24.00	3.17
CO_2 + H_2O	353.15	13.8	21	0.0015	-3.56	-24.07	3.17
CO_2 + H_2O	353.15	13.8	26	0.0017	-3.39	-22.92	3.17
CO_2 + H_2O	353.15	13.8	31	0.0016	-3.39	-22.92	3.17
CO_2 + H_2O	353.15	13.8	42	0.0016	-3.04	-20.55	3.17
CO_2 + H_2O	353.15	13.8	73	0.0016	-3.20	-21.63	3.17
CO_2 + H_2O	373.15	6.0	42	0.0010	-3.42	-24.43	3.34
CO_2 + H_2O	353.15	6.0	42	0.00077	-3.77	-25.49	3.28
CO_2 + H_2O	333.15	6.0	42	0.00071	-4.56	-29.08	3.22
CO_2 + H_2O	325.15	6.0	42	0.00056	-4.69	-29.19	3.18
CO_2 + H_2O	373.15	10.0	42	0.0013	-2.96	-21.14	3.24
CO_2 + H_2O	353.15	10.0	42	0.0012	-3.55	-24.00	3.20
CO_2 + H_2O	333.15	10.0	42	0.0010	-3.93	-25.06	3.15
CO_2 + H_2O	323.15	10.0	42	0.00081	-4.38	-27.10	3.10
CO_2 + H_2O	373.15	13.8	73	0.0017	-3.29	-23.50	3.20
CO_2 + H_2O	333.15	13.8	73	0.0012	-3.93	-26.57	3.12
CO_2 + H_2O	323.15	13.8	73	0.0010	-3.97	-25.32	3.08

a: values were obtained by PHREEQC 3.0 and corresponded to 20 min elapsed time

b: *p*H values of the (CO_2 + H_2O) system were obtained using model of Peng *et.al* [55] for the bulk solution at the start of the dissolution process.

Table 1: Calcite dissolution rate *r* in the (CO_2 + H_2O) for three pre-treated calcite samples at 353 K and 13.8 MPa.

Sample	Surface treatment	elapsed time (min)	Dissolution rate ($mol \cdot m^{-2} \cdot s^{-1}$)	Saturation Index (SI)	ΔG ($kJ \cdot mol^{-1}$)
1	Polished-perfect	20	0.0015	-4.3	-29
2	Polished-minor defect	20	0.0015	-4.1	-28
3	After 10 min elapsed time	10	0.0014	-4.7	-32

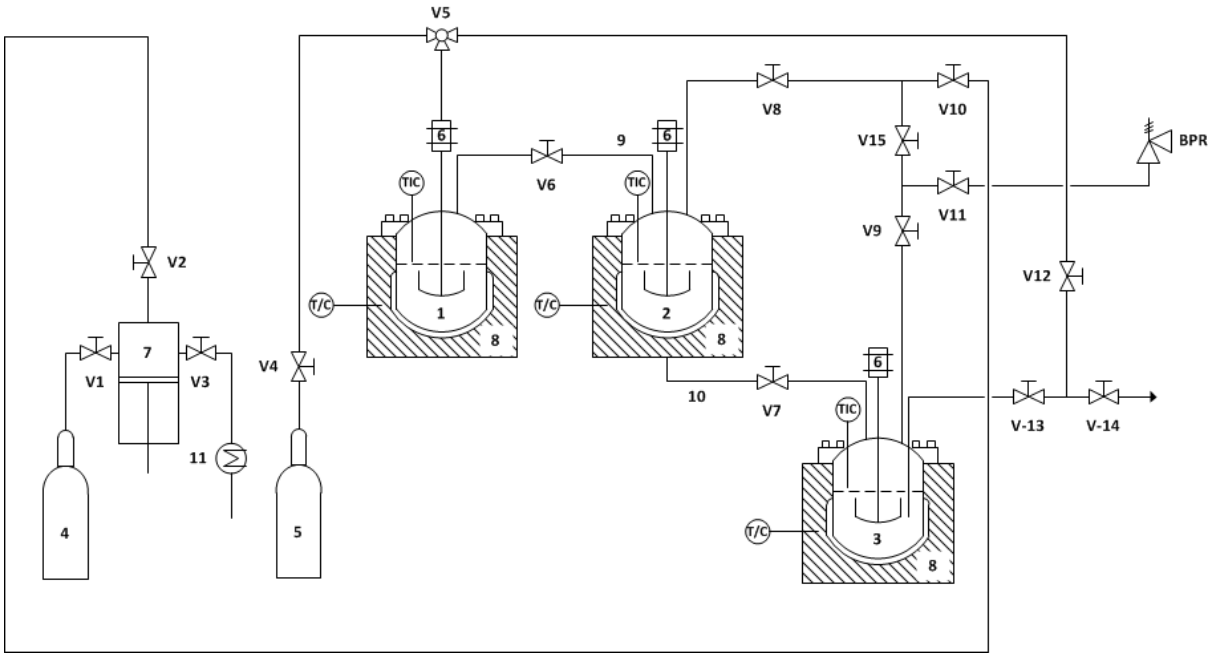

Figure 1. Schematic of the batch dissolution reactor system: 1, Reactor 1; 2, Reactor 2; 3, Reactor 3; 4, CO_2 Cylinder; 5, N_2 Cylinder; 6, Magnetic Driven Stirrer; 7, Syringe Pump; 8, Heating Jacket; 9, Liquid Transfer Line 1; 10; Liquid Transfer Line 2; 11, Chiller. Experiments in this study used only reactors 2 and 3.

Figure 2. Left, end view of the rotating disc with two calcite crystals in place. Right, view of the rotating disc system in reactor 3: 1, sampling line; 2, stirrer blades; 3, sample rock holder; 4, magnetic drive for internal stirrer.

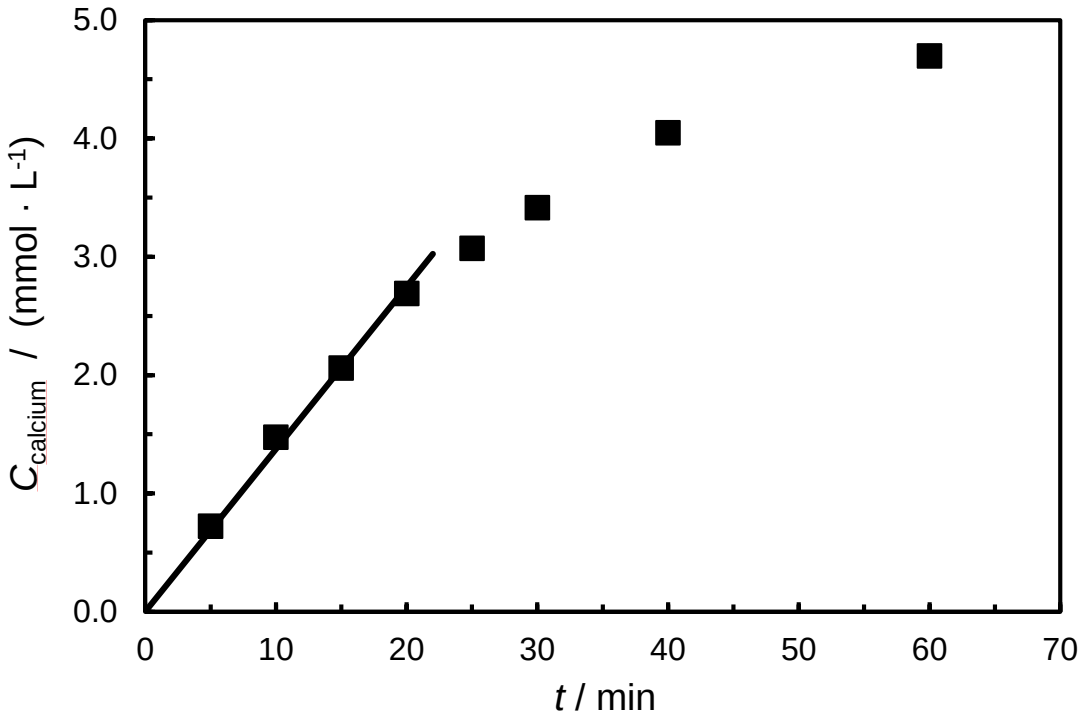

Figure 3: Concentration-time profile $c(t)$ of calcite dissolution in HCl solution at T = 353 K. The heavy line shows the linear regression for $t \leq$ 20 min from which the initial slope was determined.

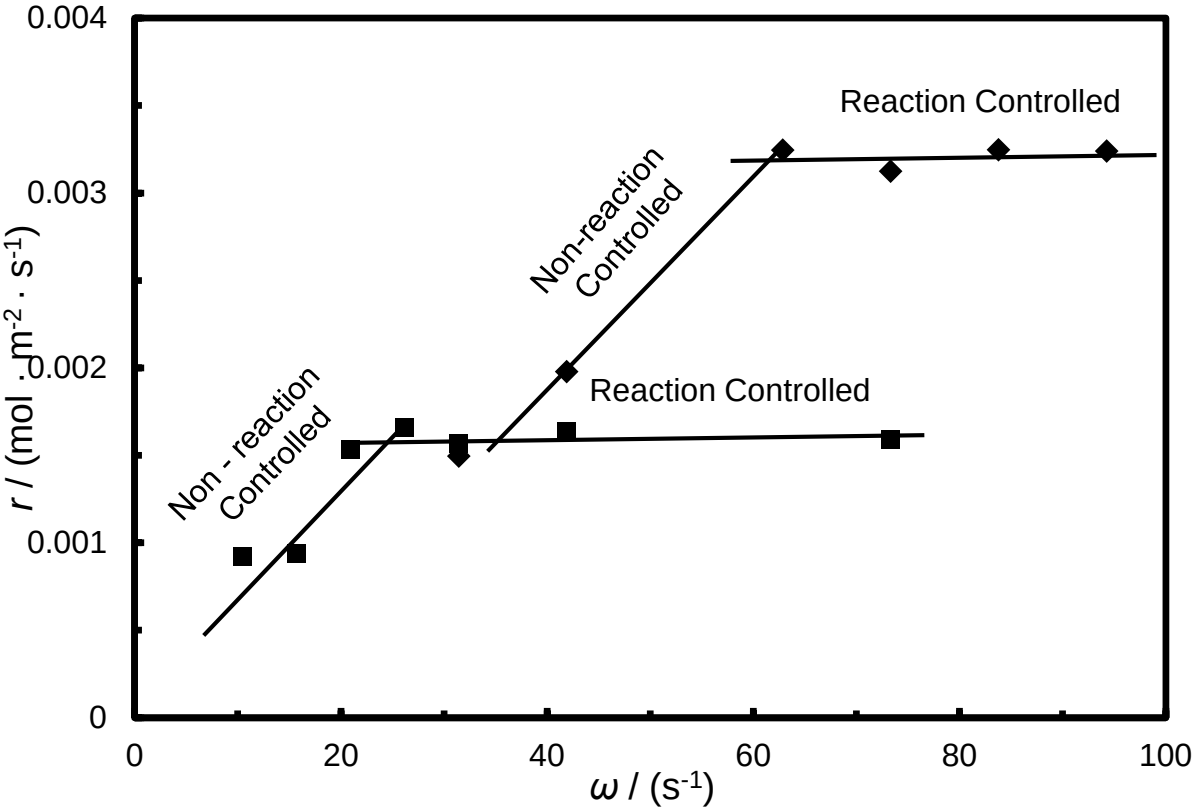

Figure 4: Calcite dissolution rate r as a function of sample angular velocity ω: ■, calcite dissolution in the (CO_2 + H_2O) system at T = 353 K and p = 13.8 MPa; ◆, calcite dissolution in 0.01 M HCl system at T = 353 K. The experimental uncertainties are comparable to the size of the plotting symbols.

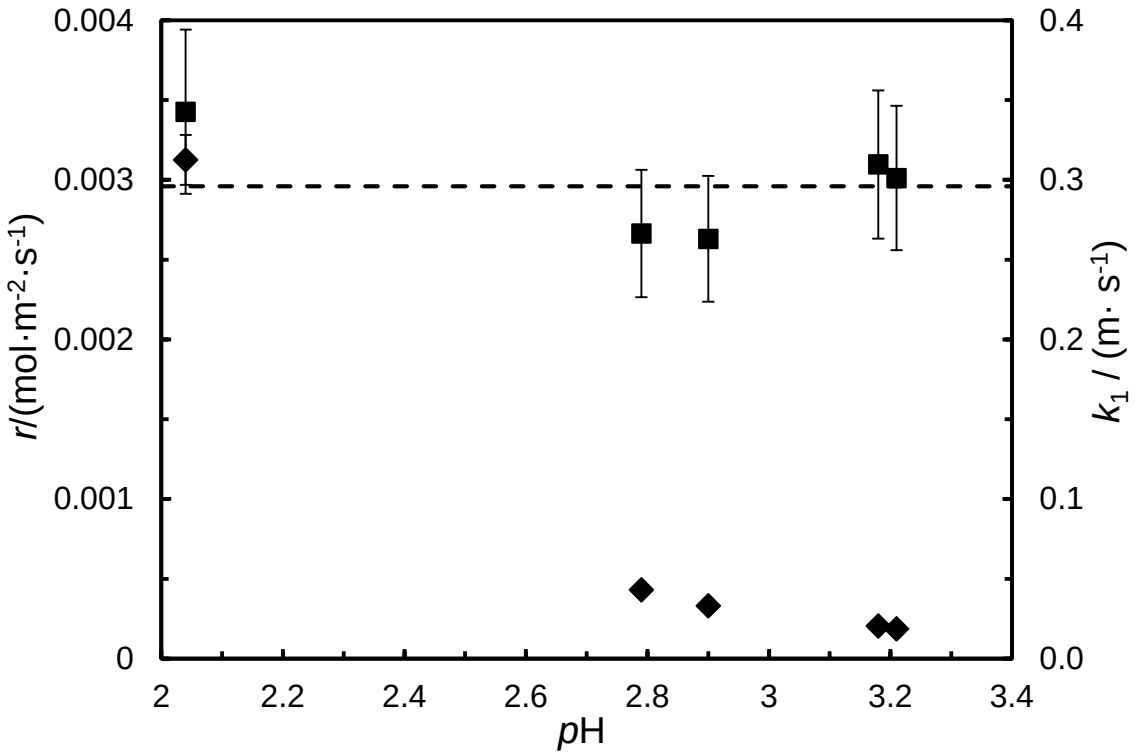

Figure 5. Reaction rate r and reaction rate constant k_1 for calcite dissolution in HCl(aq) at T = 353 K as a function of solution pH:◆, reaction rate r; ■, reaction rate constant k_1; dashed line, mean value of k_1.

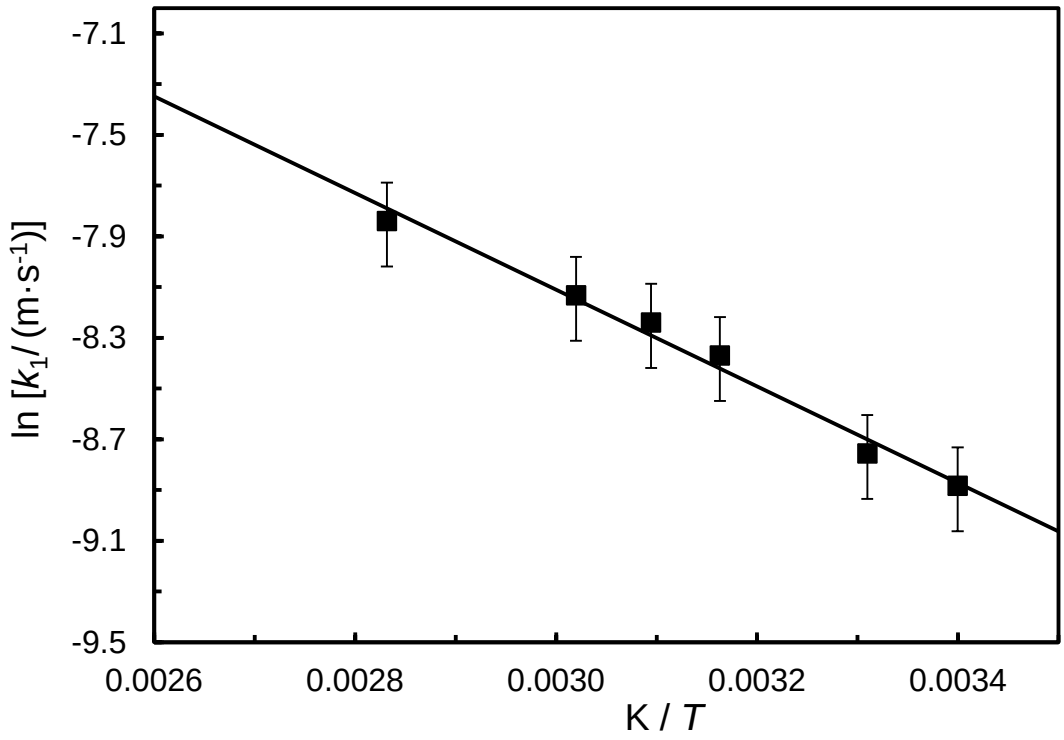

Figure 6. The effect of temperature T on reaction rate constant k_1 in the absence of CO_2: ■, experimental data. The error bars represent the expanded uncertainty of the lnk_1 values determined in this work. Solid line shows the linear regression to obtain the activation energy.

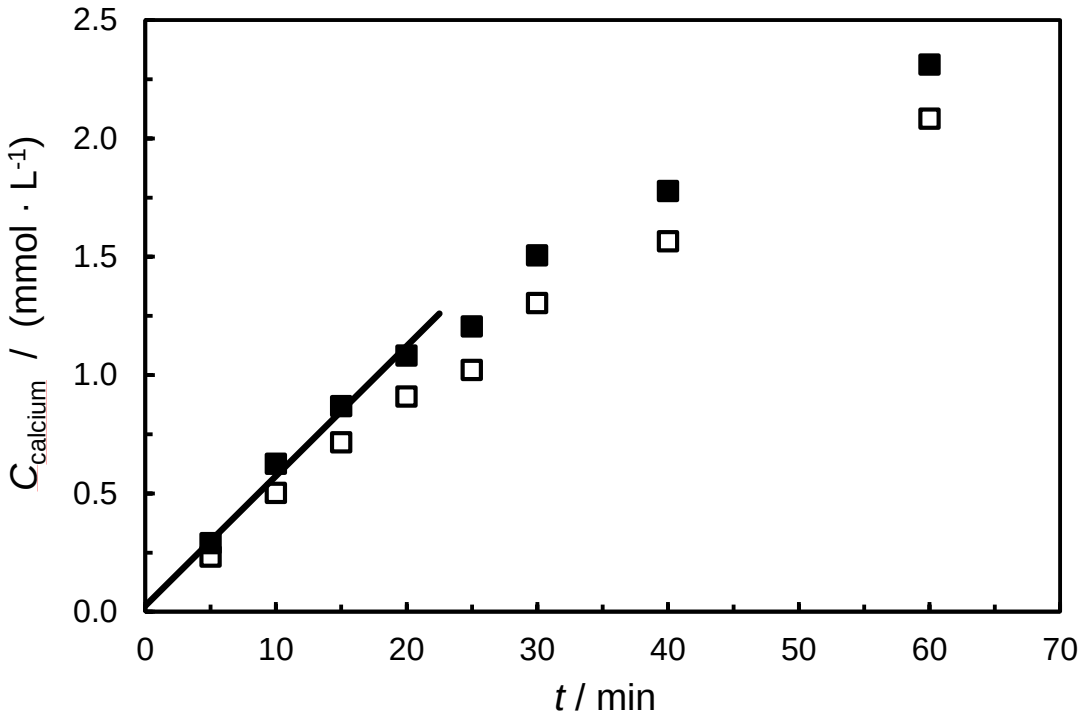

Figure 7: Concentration-time profile $c(t)$ of calcite dissolution at T = 353 K and p = 13.8 MPa. The heavy line shows the linear regression for $t \leq$ 20 min from which the initial slope was determined. The hollow points represent the uncorrected concentration obtained from the IC while the solid points correspond to the re-calculated dissolved amount incorporating the *p*H change.

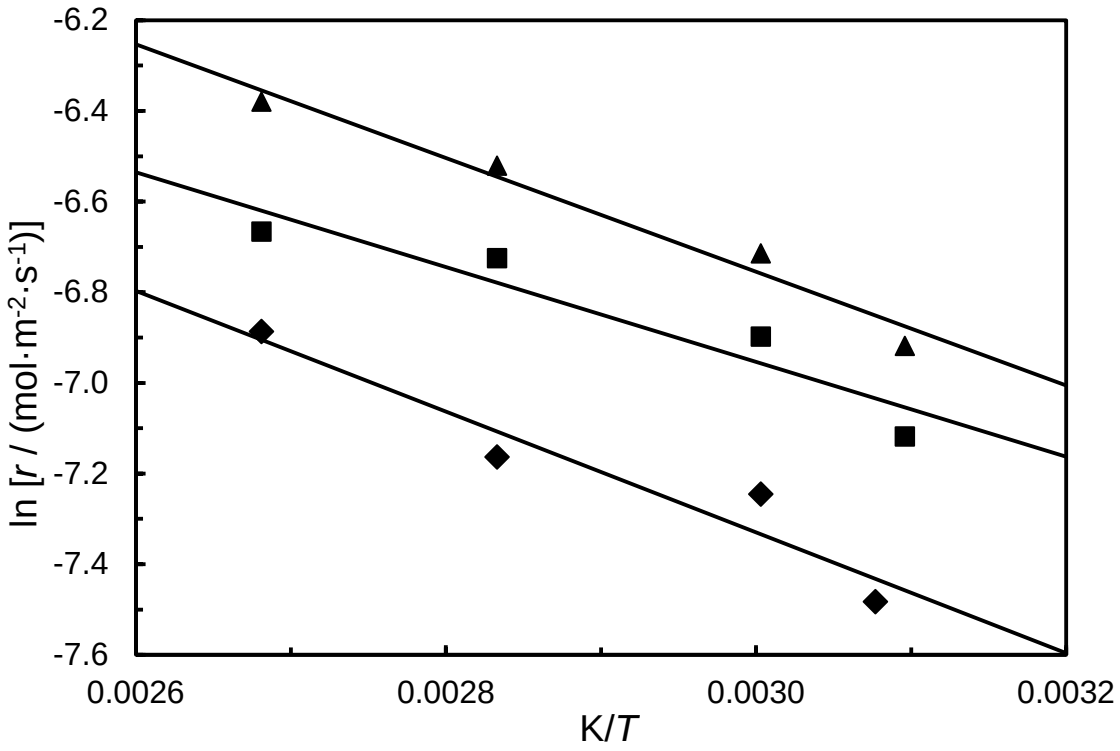

Figure 8: Calcite dissolution rate in the (CO_2 + H_2O) system as a function of temperature T:◆, p = 6 MPa; ■, p = 10 MPa; ▲, p = 13.8 MPa. The experimental uncertainties are comparable to the size of the plotting symbols. Solid lines show linear regressions.

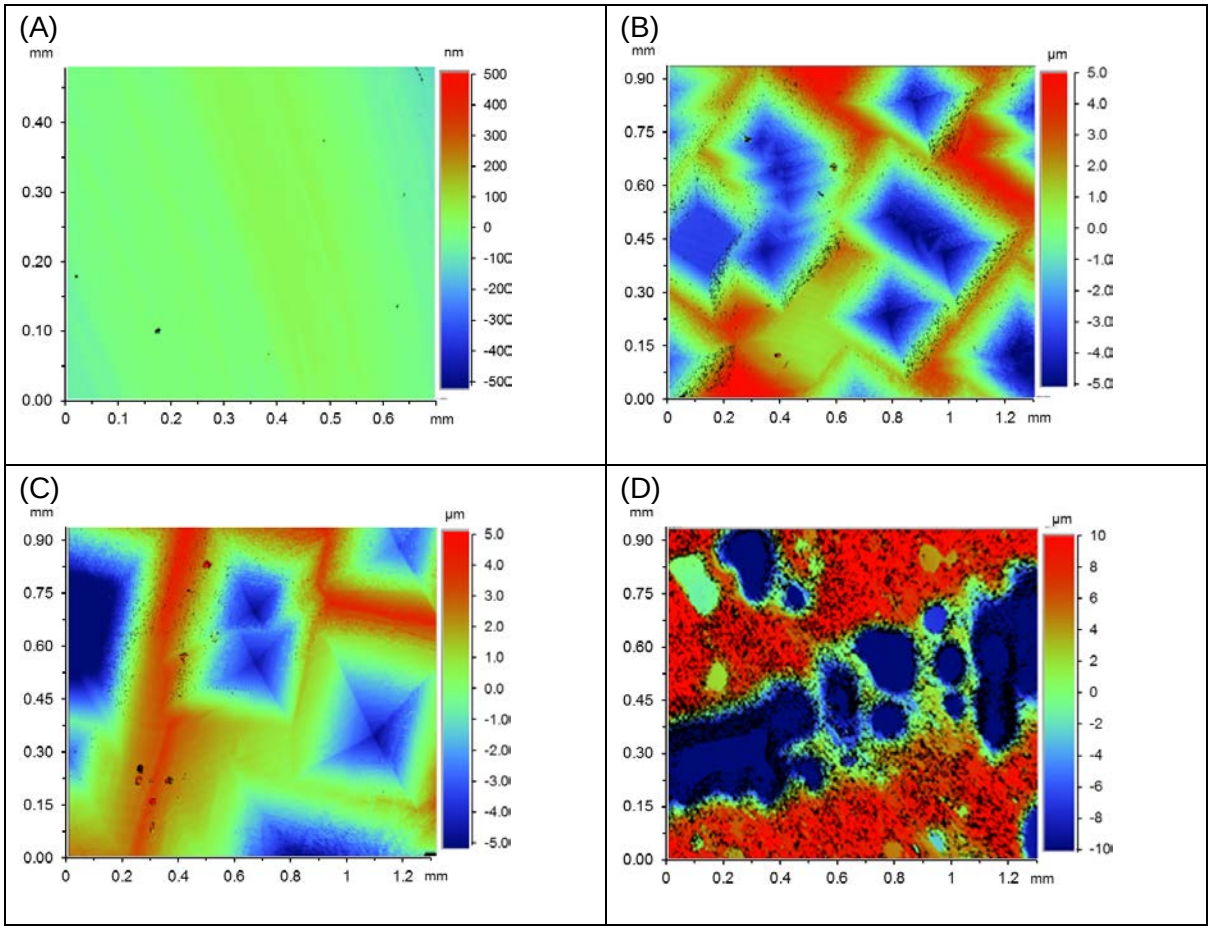

Figure 9. Vertical scanning interferometry images of calcite surfaces before and after reaction in (CO_2 + H_2O) system at T = 353 K and p = 13.8 MPa: (A) before reaction; (B) after 10 min elapsed time; (C) after 20 min elapsed time; (D) after 60 min elapsed time;

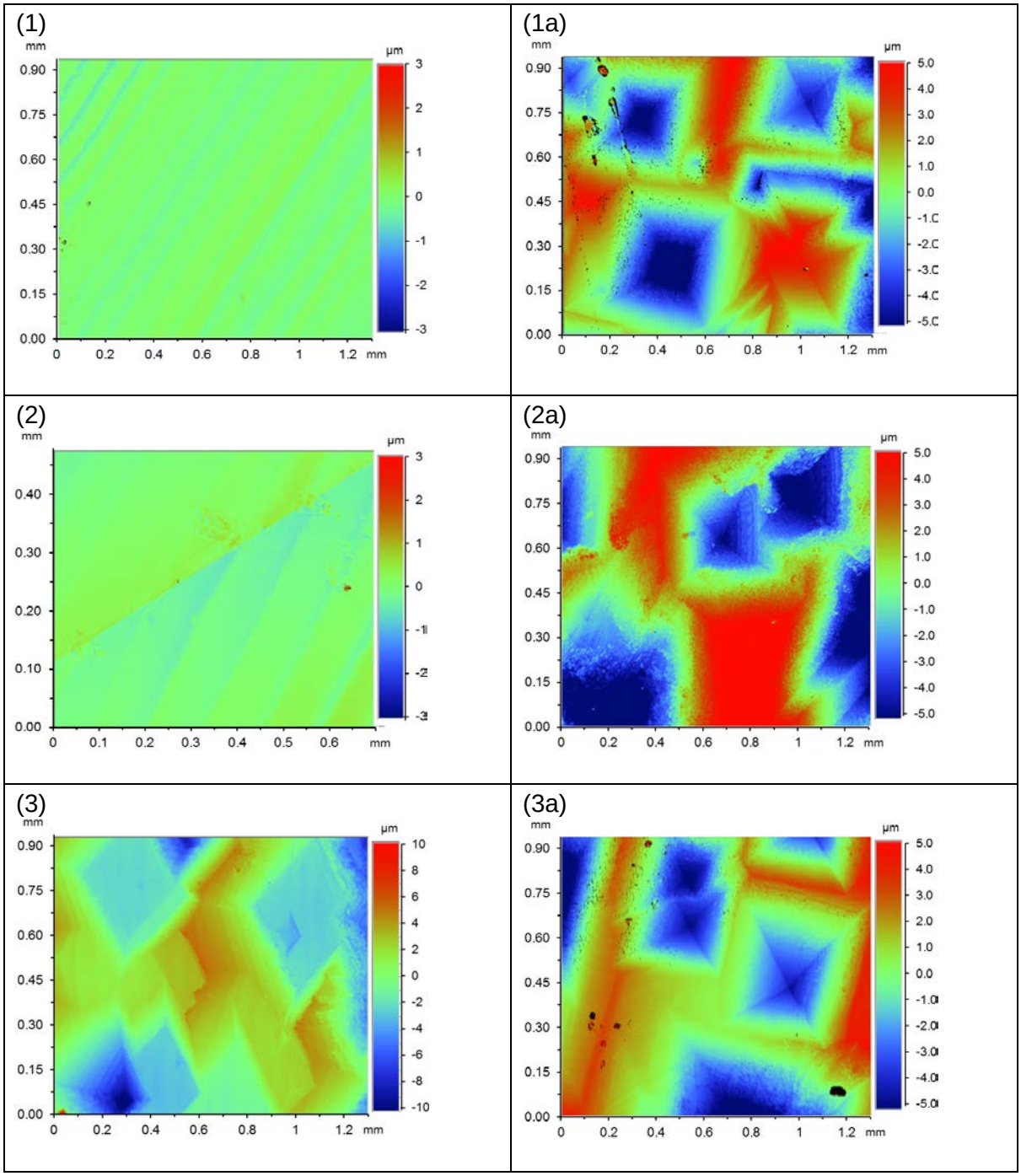

Figure 10. Effect of initial surface texture on vertical scanning interferometry images of calcite surfaces before and after reaction in (CO_2 + H_2O) system at T = 353 K and p = 13.8 MPa: (1) Sample 1 before reaction; (2) sample 2 before reaction. (3) Sample 3 before reaction; (1a) Sample 1 after 20 min elapsed time; (2a) Sample 2 after 20 min elapsed time. (3a) Sample 3 after 10 min elapsed time;

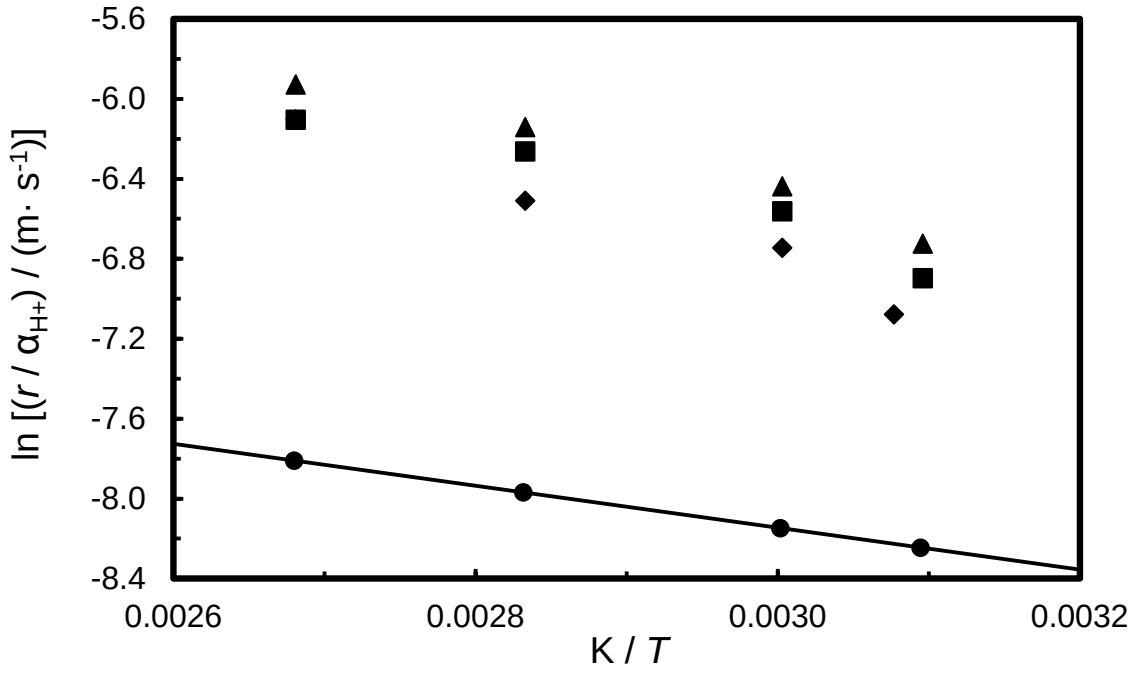

Figure 11. Relationship between $\ln(r / \alpha_{H^+})$ and $1/T$ in the (CO_2 + H_2O) system: ◆, p = 6 MPa; ■, p = 10 MPa; ▲, p = 13.8 MPa. Also ●, k_1 for calcite dissolution in the (HCl + H_2O) system. The experimental uncertainties are comparable to the size of the plotting symbols.

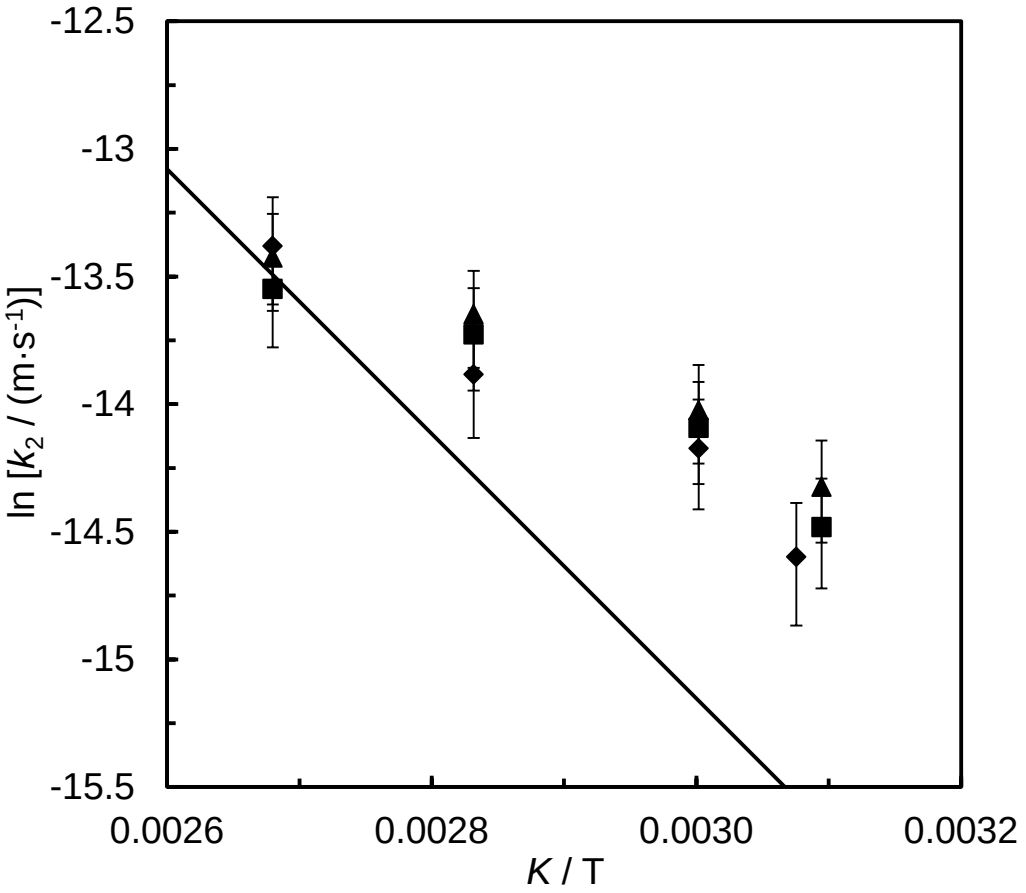

Figure 12. The effect of temperature T on the reaction rate constant k_2 for the reaction between calcite and H_2CO_3* in the (CO_2 + H_2O) system at pressures of (6.0, 10.0 and 13.8) MPa. ◆, p = 6 MPa; ■, p = 10 MPa; ▲, p = 13.8 MPa. The error bars represent the expanded uncertainty of the ln*k2* values determined in this work. Solid line shows the linear regression to obtain the activation energy.

REFERENCES

[1] M. Blunt, Carbon dioxide storage - Briefing paper no 4, in: Grantham Institute of Climate Change, Imperial College London, UK, 2010.

[2] S. Bachu, Sequestration of CO2 in geological media: criteria and approach for site selection in response to climate change, Energy Conversion and Management, 41 (2000) 953-970.

[3] K.L. Anthonsen, P. Aagaard, P.E.S. Bergmo, M. Erlström, J.I. Fareide, S.R. Gislason, G.M. Mortensen, S.Ó. Snæbjörnsdottir, CO2 Storage Potential in the Nordic Region, Energy Procedia, 37 (2013) 5080-5092.

[4] R.B. Grigg, R.K. Svec, P.C. Lichtner, W. Carey, C.E. Lesher, CO2/Brine/Carbonate rock interactions: dissolution and precipitation in: Fourth Annual Conference on Carbon Capture & Sequestration, Alexandria, Virginia, 2005.

[5] P. Egermann, B. Bazin, V. O, An experimental investigation of reaction -transport phenomena during CO2 injection, in: SPE Middle East Oil and Gas Show and Conference, Kingdom of Bahrain, 2005.

[6] A. Al-Siddiqi, R.A. Dawe, QATAR'S OIL AND GASFIELDS: A REVIEW, Journal of Petroleum Geology, 22 (1999) 417-436.

[7] J.P. Kaszuba, D.R. Janecky, M.G. Snow, Carbon dioxide reaction processes in a model brine aquifer at 200 °C and 200 bars: implications for geologic sequestration of carbon, Applied Geochemistry, 18 (2003) 1065-1080.

[8] H. Koide, Y. Shindo, Y. Tazaki, M. Iijima, K. Ito, N. Kimura, K. Omata, Deep sub-seabed disposal of CO2 — The most protective storage —, Energy Conversion and Management, 38, Supplement (1997) S253-S258.

[9] I.M. Mohamed, J. He, H.A. Nasr-El-Din, Permeability Change during CO2 injection in Carbonate Rock: A Coreflood Study, in: SPE Production and Operations Symposium, Oklahoma City, Oklahoma, USA, 2011.

[10] M.L. Druckenmiller, M.M. Maroto-Valer, Carbon sequestration using brine of adjusted pH to form mineral carbonates, Fuel Processing Technology, 86 (2005) 1599-1614.

[11] M.M. Reddy, L.N. Plummer, E. Busenberg, Crystal growth of calcite from calcium bicarbonate solutions at constant PCO2 and 25°C: a test of a calcite dissolution model, Geochimica et Cosmochimica Acta, 45 (1981) 1281-1289.

[12] J.W. Morse, R.S. Arvidson, The dissolution kinetics of major sedimentary carbonate minerals, Earth-Science Reviews, 58 (2002) 51-84.

[13] R.A. Berner, J.W. Morse, Dissolution kinetics of calcium carbonate in seawater: IV. Theory of calcite dissolution, Am. J. Sci., 274 (1974) 108–134.

[14] L.N. Plummer, T.M.L. Wigley, The dissolution of calcite in CO2-saturated solutions at 25°C and 1 atmosphere total pressure, Geochimica et cosmochimica acta, 40 (1976) 191-202.

[15] L.N. Plummer, T.M.L. Wigley, D.L. Parkhurst, The kinetics of calcite dissolution in CO 2 - water systems at 5 degrees to 60 degrees C and 0.0 to 1.0 atm CO 2, American Journal of Science, 278 (1978) 179-216.

[16] E.L. Sjöberg, A fundamental equation for calcite dissolution kinetics, Geochimica et Cosmochimica Acta, 40 (1976) 441-447.

[17] R. Wollast, Rate and mechanism of dissolution of carbonates in the system CaCO3 – MgCO3, Wiley, Aquatic Chemical Kinetics, 1990.

[18] J.W. Morse, J. De Kanel, K. Harris, Dissolution kinetics of calcium carbonate in seawater: VII. The dissolution kinetics of aragonite and pteropod tests. , Am. J. Sci., 279 (1979) 488-502.

[19] Y.O. Rosenberg, I.J. Reznik, S. Zmora-Nahum, J. Ganor, The effect of pH on the formation of a gypsum scale in the presence of a phosphonate antiscalant, Desalination, 284 (2012) 207-220.

[20] I.N. MacInnis, S.L. Brantley, The role of dislocations and surface morphology in calcite dissolution, Geochimica et cosmochimica acta, 56 (1992) 1113-1126.

[21] K.M. Hung, A.D. Hill, K. Sepehrnoori, A mechanistic model of wormhole growth in carbonate matrix acidizing and acid fracturing, Journal of Petroleum Technology, 41 (1989) 59-66.

[22] S.J. Tinker, Equilibrium acid fracturing. A new fracture acidizing technique for carbonate formations, SPE Production Engineering, 6 (1989) 25-32.

[23] S.L. Brantley, Kinetics of mineral dissolution, in: Kinetics of water-rock interaction, Springer, 2008, pp. 151-210.

[24] L. Chou, R.M. Garrels, R. Wollast, Comparative study of the kinetics and mechanisms of dissolution of carbonate minerals, Chemical Geology, 78 (1989) 269-282.
[25] R.G. Compton, K.L. Pritchard, P.R. Unwin, The dissolution of calcite in acid waters: mass transport versus surface control, Freshwater Biology, 22 (1989) 285–288.
[26] O.S. Pokrovsky, S.V. Golubev, J. Schott, A. Castillo, Calcite, dolomite and magnesite dissolution kinetics in aqueous solutions at acid to circumneutral pH, 25 to 150 °C and 1 to 55 atm pCO2: New constraints on CO2 sequestration in sedimentary basins, Chemical Geology, 265 (2009) 20-32.
[27] O.S. Pokrovsky, S.V. Golubev, J. Schott, Dissolution kinetics of calcite, dolomite and magnesite at 25 °C and 0 to 50 atm pCO2, Chemical Geology, 217 (2005) 239-255.
[28] J.W. Morse, R.S. Arvidson, A. Lüttge, Calcium carbonate formation and dissolution, Chemical reviews, 107 (2007) 342-381.
[29] V.G. Levitch, Physicochemical Hydrodynamics, in, Prentice-Hall Inc, 1962.
[30] M. Alkattan, E.H. Oelkers, J.-L. Dandurand, J. Schott, Experimental studies of halite dissolution kinetics: II. The effect of the presence of aqueous trace anions and K3Fe(CN)6, Chemical Geology, 143 (1997) 17-26.
[31] D.P. Gregory, A.C. Riddiford, 731. Transport to the surface of a rotating disc, Journal of the Chemical Society (Resumed), 0 (1956) 3756-3764.
[32] C.N. Fredd, H. Scott Fogler, The kinetics of calcite dissolution in acetic acid solutions, Chemical Engineering Science, 53 (1998) 3863-3874.
[33] K. Lund, H.S. Fogler, C.C. McCune, J.W. Ault, Acidization—II. The dissolution of calcite in hydrochloric acid, Chemical Engineering Science, 30 (1975) 825-835.
[34] R.A. Berner, G.R. Holdren Jr, Mechanism of feldspar weathering—II. Observations of feldspars from soils, Geochimica et Cosmochimica Acta, 43 (1979) 1173-1186.
[35] O.W. Duckworth, S.T. Martin, Dissolution rates and pit morphologies of rhombohedral carbonate minerals, American Mineralogist, 89 (2004) 554-563.
[36] J. Xu, C. Fan, H.H. Teng, Calcite dissolution kinetics in view of Gibbs free energy, dislocation density, and pCO2, Chemical Geology, 322–323 (2012) 11-18.
[37] A. Lüttge, Crystal dissolution kinetics and Gibbs free energy, Journal of Electron Spectroscopy and Related Phenomena, 150 (2006) 248-259.
[38] C. Fischer, R.S. Arvidson, A. Lüttge, How predictable are dissolution rates of crystalline material?, Geochimica et Cosmochimica Acta, 98 (2012) 177-185.
[39] O.W. Duckworth, S.T. Martin, Connections between surface complexation and geometric models of mineral dissolution investigated for rhodochrosite, Geochimica et Cosmochimica Acta, 67 (2003) 1787-1801.
[40] R.S. Arvidson, I.E. Ertan, J.E. Amonette, A. Luttge, Variation in calcite dissolution rates:: A fundamental problem?, Geochimica et cosmochimica acta, 67 (2003) 1623-1634.
[41] J. Schott, E.H. Oelkers, P. Bénézeth, Y. Goddéris, L. François, Can accurate kinetic laws be created to describe chemical weathering?, Comptes Rendus Geoscience, 344 (2012) 568-585.
[42] C. Noiriel, L. Luquot, B. Madé, L. Raimbault, P. Gouze, J. Van Der Lee, Changes in reactive surface area during limestone dissolution: An experimental and modelling study, Chemical Geology, 265 (2009) 160-170.
[43] M.H. Al-Khaldi, H.A. Nasr-El-Din, H.K. Sarma, Kinetics of the reaction of citric acid with calcite, in: SPE International Symposium on Oilfield Chemistry, Society of Petroleum Engineers, 2009.
[44] O. Gundogan, E. Mackay, A. Todd, Comparison of numerical codes for geochemical modelling of CO< sub> 2</sub> storage in target sandstone reservoirs, Chemical Engineering Research and Design, 89 (2011) 1805-1816.
[45] H. Hellevang, V.T. Pham, P. Aagaard, Kinetic modelling of CO< sub> 2</sub>–water–rock interactions, International Journal of Greenhouse Gas Control, 15 (2013) 3-15.
[46] D. Buhmann, W. Dreybrodt, Calcite dissolution kinetics in the system H2O CO2 CaCO3 with participation of foreign ions, Chemical Geology, 64 (1987) 89-102.
[47] M. Alkattan, E.H. Oelkers, J.-L. Dandurand, J. Schott, An experimental study of calcite and limestone dissolution rates as a function of pH from −1 to 3 and temperature from 25 to 80°C, Chemical Geology, 151 (1998) 199-214.

[48] E.L. Sjöberg, D.T. Rickard, Temperature dependence of calcite dissolution kinetics between 1 and 62 C at pH 2.7 to 8.4 in aqueous solutions, Geochimica et Cosmochimica Acta, 48 (1984) 485-493.
[49] A. Gutjahr, H. Dabringhaus, R. Lacmann, Studies of the growth and dissolution kinetics of the CaCO< sub> 3</sub> polymorphs calcite and aragonite I. Growth and dissolution rates in water, Journal of crystal growth, 158 (1996) 296-309.
[50] D.W. Finneran, J.W. Morse, Calcite dissolution kinetics in saline waters, Chemical Geology, 268 (2009) 137-146.
[51] D.K. Gledhill, J.W. Morse, Calcite dissolution kinetics in Na–Ca–Mg–Cl brines, Geochimica et Cosmochimica Acta, 70 (2006) 5802-5813.
[52] T. Arakaki, A. Mucci, A continuous and mechanistic representation of calcite reaction-controlled kinetics in dilute solutions at 25°C and 1 atm total pressure, Aquat Geochem, 1 (1995) 105-130.
[53] E.L. Sjöberg, D.T. Rickard, Calcite dissolution kinetics: Surface speciation and the origin of the variable pH dependence, Chemical Geology, 42 (1984) 119-136.
[54] J.R. Ruaya, T.M. Seward, The ion-pair constant and other thermodynamic properties of HCl up to 350°C, Geochimica et Cosmochimica Acta, 51 (1987) 121-130.
[55] C. Peng, J.P. Crawshaw, G.C. Maitland, J.P. Martin Trusler, D. Vega-Maza, The pH of CO2-saturated water at temperatures between 308 K and 423 K at pressures up to 15 MPa, The Journal of Supercritical Fluids, 82 (2013) 129-137.
[56] L.N. Plummer, E. Busenberg, The solubilities of calcite, aragonite and vaterite in CO2-H2O solutions between 0 and 90°C, and an evaluation of the aqueous model for the system CaCO3-CO2-H2O, Geochimica et cosmochimica acta, 46 (1982) 1011-1040.
[57] S.-X. Hou, G.C. Maitland, J.P.M. Trusler, Measurement and modeling of the phase behavior of the (carbon dioxide plus water) mixture at temperatures from 298.15 K to 448.15 K, The Journal of Supercritical Fluids, 73 (2013) 87-96.
[58] R. Shiraki, P. Rock, W. Casey, Dissolution Kinetics of Calcite in 0.1 M NaCl Solution at Room Temperature: An Atomic Force Microscopic (AFM) Study, Aquat Geochem, 6 (2000) 87-108.
[59] R.S. Arvidson, A. Luttge, Mineral dissolution kinetics as a function of distance from equilibrium – New experimental results, Chemical Geology, 269 (2010) 79-88.
[60] H.H. Teng, Controls by saturation state on etch pit formation during calcite dissolution, Geochimica et cosmochimica acta, 68 (2004) 253-262.
[61] A.E. Blum, R.A. Yund, A.C. Lasaga, The effect of dislocation density on the dissolution rate of quartz, Geochimica et Cosmochimica Acta, 54 (1990) 283-297.
[62] J. Schott, S. Brantley, D. Crerar, C. Guy, M. Borcsik, C. Willaime, Dissolution kinetics of strained calcite, Geochimica et Cosmochimica Acta, 53 (1989) 373-382.
[63] Z. Duan, R. Sun, An improved model calculating CO2 solubility in pure water and aqueous NaCl solutions from 273 to 533 K and from 0 to 2000 bar, Chemical Geology, 193 (2003) 257-271.
[64] J.B. Fein, J.V. Walther, Calcite solubility in supercritical CO2 H2O fluids, Geochimica et Cosmochimica Acta, 51 (1987) 1665-1673.
[65] R.H. Garrett, C.M. Grisham, Biochemistry, 5th ed., Wadsworth Publishing Co Inc, 2012.
[66] L. D.R, CRC Handbook of Chemistry and Physics, 71st ed., CRC Press, 1990.
[67] G. De Giudici, Surface control vs. diffusion control during calcite dissolution: Dependence of step-edge velocity upon solution pH, American Mineralogist, 87 (2002) 1279-1285.